Analyst

ROYAL SOCIETY OF CHEMISTRY

PAPER

View Article Online
View Journal | View Issue

Cite this: *Analyst*, 2021, **146**, 3686

Detection of trace amounts of insoluble pharmaceuticals in water by extraction and SERS measurements in a microfluidic flow regime

Vasilii Burtsev,[a] Mariia Erzina,[a,b] Olga Guselnikova,[a,b] Elena Miliutina,[a,b] Yevgeniya Kalachyova,[a] Vaclav Svorcik[a] and Oleksiy Lyutakov *[a,b]

Detection of trace amounts of poorly water-soluble pharmaceuticals or related (bio)solutions represents a key challenge in environment protection and clinical diagnostics. However, this task is complicated by low concentrations of pharmaceuticals, complex sample matrices, and sophisticated sample preparative routes. In this work, we present an alternative approach on the basis of an on-line flow extraction procedure and SERS measurements performed in a microfluidic regime. The advantages of our approach were demonstrated using ibuprofen (Ibu), which is considered as a common pharmaceutical contaminant in wastewater and should be monitored in various bioliquids. The extraction of Ibu from water to the dichloromethane phase was performed with an optimized microfluidic mixer architecture. As SERS tags, lipophilic functionalized gold multibranched nanoparticles (AuMs) were added to the organic phase. After microfluidic extraction, Ibu was captured by the functionalized AuM surface and recognized by on-line SERS measurements with up to 10−8 M detection limit. The main advantages of the proposed approach can be regarded as its simplicity, lack of need for preliminary sample preparation, high reliability, the absence of sample pretreatment, and low detection limits.

Received 8th December 2020,
Accepted 15th April 2021

DOI: 10.1039/d0an02360d

rsc.li/analyst

Introduction

Due to the active consumption of medicines by humanity, pharmaceutical compounds increasingly pollute the environment and pose a serious risk to ecological safety.[1,2] In particular, widely used pharmaceuticals are commonly detected in the natural aquatic environment at concentrations from subnano- to micrograms per liter. Their poor biodegradability and high bioactivity represent a high risk for environmental ecosystems.[3–5] One of the key issues aimed at the monitoring and prevention of pharmaceutical-related aqueous contamination lies in the development of sensitive, reliable, and rapid methods of pharmaceutical detection in water, including samples with complex compositions.[6–8]

In the field of pharmaceutical identification and detection, the most common methods are different chromatographic approaches coupled with mass-spectrometry or various electrochemical methods.[9,10] Indeed, these analytical routes show excellent results in the case of preliminary treated water, but their application to "real" wastewater samples is highly questionable, due to the presence of signals from interfering substances, which lead to poor signal resolution and high analytical errors.[11] In addition, the utilization of chromatographic detection methods is restricted by time throughput and bulky instrumentation.[12–14] An alternative approach consists of the utilization of the surface-enhanced Raman spectroscopy (SERS) method, which is favoured by unprecedented sensitivity leading to very low detection limits.[15–20] However, common SERS substrates do not show sufficient specificity towards the targeted analytes and, like chromatography or electrochemical techniques, they are almost useless in the case of complex wastewater samples without their previous purification/separation. This drawback is usually overcome through the functionalization of the SERS-active surfaces, allowing solid-state microextraction directly onto the SERS surface and selection/detection of targeted molecules with a high degree of reliability and specificity.[21–24] In this regard, especially attractive is the utilization of a lab-on-a-chip based SERS approach, which allows us to perform several analytical procedures (sample dosage, extraction, and identification) in the framework of a single chip and makes the analytical procedures portable and mobile.[25–29] One of the first attempts to introduce the microfluidic SERS approach is reported in ref. 30. More recent works are focused on the detection of trace amounts of drugs in complex matrices with as much as possible high reliability and low detection

[a]*Department of Solid State Engineering, Institute of Chemical Technology, 16628 Prague, Czech Republic. E-mail: lyutakoo@vscht.cz*
[b]*Research School of Chemistry and Applied Biomedical Sciences, Tomsk Polytechnic University, Russian Federation*

limits.[31–33] The low detection limit is commonly introduced through specific chip design or carrier fluid composition, which enhances the analyte–plasmon active nanoparticle interaction and prevents the agglomeration of nanoparticles.[30,31,34–36] In addition, varying the shape, size, and surface chemistry of nanoparticles also provides an elegant opportunity to increase the intrinsic SERS enhancement or provide higher affinity towards targeted drugs.[37–39] However, even in the analysis of complex media, the common problem, which restricts the loc-SERS utilization, is related to nanoparticle agglomeration, which can be induced by the sample medium and significantly restricts the real applicability of the methods.

In this work, we propose a detection approach aimed at the rapid and portative identification (qualitative and quantitative) of trace amounts of low water-soluble pharmaceuticals in aqueous medium. Our approach is based on the combination of a microfluidic mixer, plasmonic nanoparticles with shaped edges (for efficient light energy concentration), surface chemistry tuning (for stabilization of nanoparticles in the organic phase and enhancement of the nanoparticle surface affinity towards the targeted analyte–Ibu), and on-line SERS measurements performed in a microfluidic regime. Unlike the previously reported LoC-SERS approaches, we used plasmon-active nanoparticles, which are stabilized in the organic phase and not miscible with water. This approach allows us to measure the signal from targeted (*i.e.*, extracted in the organic phase) compounds and prevent the nanoparticle agglomeration due to the impact of the sample matrix, which often contains metal ions (commonly induced nanoparticle agglomeration).

Experimental

Materials and sample preparation

Isopropyl alcohol, methanol (≥99.9%), deionized water, dichloromethane (≥99.8%), high-purity water (EMD MILLIPORE), chloroauric acid tetrahydrate ($HAuCl_4 \cdot 4H_2O$, 99.9%), silver nitrate ($AgNO_3$, 99.0%), ascorbic acid (AA, 99.0%), N,O-bis(trimethylsilyl)trifluoroacetamide for GC derivatization, anhydrous pyridine (99.8%), anhydrous 1,4-dioxane (99.8%), ibuprofen (Pharmaceutical Standard), carbamazepine (Pharmaceutical Standard), celecoxib (Pharmaceutical Standard), humic acid, calcium chloride dihydrate (≥99%), calcium hydroxide (≥95.0%), magnesium chloride hexahydrate (≥99%), calcium sulfate dihydrate (≥98%), sodium chloride (≥99%), magnesium sulfate heptahydrate (≥99%), potassium chloride (≥99%), magnesium oxide (≥97%), sodium bicarbonate (≥99.5%), sodium sulfate (≥99%), sodium fluoride (≥99%), potassium bicarbonate (≥99.5%), sodium bromide (≥99%), sodium nitrate (≥99%), strontium chloride (≥99.99%), sodium phosphate monobasic (≥99%), potassium phosphate dibasic (≥98%), potassium carbonate (≥99%), and iron(II) sulfate heptahydrate (≥99%) were purchased from Sigma-Aldrich and used without further purification.

3D microfluidic chips were fabricated from Clear resin (Formlabs, USA) and covered with optically transparent, 0.2 mm thick glass (Hirschmann, Germany). The 4-hexadecyl benzene diazonium tosylate (ADT-$C_{16}H_{33}$) salt was prepared and grafted to the SERS-active surface according to the procedure reported in ref. 40. Briefly, diazotization was performed using a polymer-supported diazotization agent in the presence of *p*-toluenesulfonic acid.

Artificial freshwater and wastewater were synthesized using a seed-mediated method according to a previously published procedure, respectively.[41,42] Surface water was prepared using a 100 ppm humic acid solution in distilled water in accordance with previously published methods.[43,44]

Sample preparation

The microfluidic chip was made using 3D printing (the model is shown in Fig. 1). The model for printing was designed in the program COMSOL Multiphysics. After preparation, the

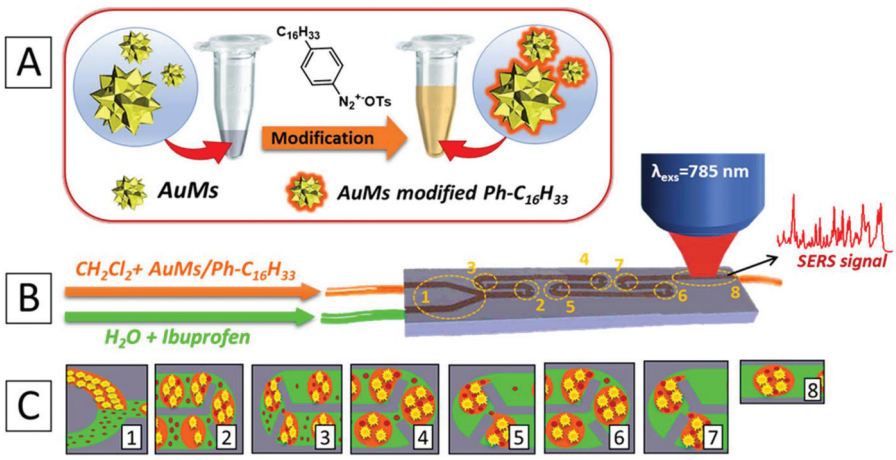

Fig. 1 (A) Graphical depiction of AuMs and AuMs surface grafting with Ph-$C_{16}H_{33}$ for increasing their stability in dichloromethane; (B) schematic representation of the microfluidic chip for Ibu on-line extraction and SERS identification; and (C) details of the experimental set-up (1–8 position on the chip).

microfluidic chip was washed with isopropyl, dried at 50 °C for 12 h, and irradiated with a UV-source for 2 h. Finally, the chip surface was covered with thin (100 μm) microscopic glass, carefully stuck to the chip surface.

Gold multibranched nanoparticles (AuMs) were synthesized using a seed-mediated method according to a previously published procedure.[45] Briefly, aqueous $HAuCl_4$ solution (100 mL, 10 mm) was mixed with deionized water (3 mL), and then aqueous $AgNO_3$ solution (6 mL, 10 mm) was added under magnetic stirring for 30 s. After the solutions had been thoroughly mixed, ascorbic acid (2 mL, 100 mm) was "quickly" added, and the solution was stirred vigorously for 10 s at room temperature (RT). The prepared AuMs were dispersed in water (3 mL) and were purified three times by centrifugation. For further use, the resultant precipitates were redissolved in deionized water.

The modification of the AuM surface was performed in a spontaneous way. 1 ml of as-prepared AuMs was mixed with 2 ml of 6 mM freshly prepared methanol solution of ADT-$C_{16}H_{33}$ under stirring for 45 min. After the modification, the AuMs were rinsed with methanol and acetone and dried under ambient conditions. The procedure of AuM rinsing/drying was repeated three times. In the final step, the grafted AuMs were dispersed in dichloromethane.

For control experiments (gas chromatography (GS)), ibuprofen (Ibu) was derivatized with *N*,*O*-bis(trimethylsilyl) trifluoroacetamide by dissolving Ibu powder (or extracted Ibu) in a mixture of 500 μl of *N*,*O*-bis(trimethylsilyl) trifluoroacetamide, and 500 μl of pyridine, and keeping at 50 °C for 3 h. Carbamazepine (CBZ) was derivatized with *N*,*O*-bis(trimethylsilyl) trifluoroacetamide by dissolving CBZ powder (or extracted CBZ) in a mixture of 500 μl of *N*,*O*-bis(trimethylsilyl) trifluoroacetamide and 500 μl of pyridine, and keeping at 60 °C for 3 h. Celecoxib (Cel) was derivatized with *N*,*O*-bis(trimethylsilyl) trifluoroacetamide by dissolving Cel powder (or extracted Cel) in a mixture of 500 μl of *N*,*O*-bis(trimethylsilyl) trifluoroacetamide and 500 μl of 1,4-dioxane, and keeping at 60 °C for 3 h.

Measurement techniques

Transmission electron microscopy (TEM) images were obtained with a JEOL JEM1010 instrument (JEOL Ltd, Japan). UV-Vis absorption spectra were recorded using a Lambda 25 UV/vis/NIR spectrometer (PerkinElmer) in a 400–1100 nm spectral range. The gas chromatographic analysis of ibuprofen, carbamazepine and celecoxib was carried out on an Agilent Technologies 8860 GC system equipped with an HP-5 column. The GC analysis of Ibu was carried out with the following parameters: splitless mode, injector and interface temperature – 270 °C, initial column temperature – 80 °C, temperature ramp – 10 °C min^{-1}, up to 300 °C. The GC analysis of CBZ was carried out with the following parameters: splitless mode, injector and interface temperature – 280 °C, initial column temperature – 90 °C, temperature ramp – 15 °C min^{-1}, up to 150 °C, temperature ramp – 5 °C min^{-1}, up to 250 °C, temperature ramp – 15 °C min^{-1}, up to 275 °C.[46–48] The GC analysis of Cel was carried out with the following parameters: splitless mode, injector and interface temperature – 305 °C, initial column temperature – 100 °C, temperature ramp – 10 °C min^{-1}, up to 300 °C.[46–48] Raman data were acquired in the microfluidic chip at ambient temperature, using a customized microfluidic device equipped with a microscopic Raman spectrometer ProRaman-L (785 nm excitation laser). The excitation power was 60 mW and conditions of measurement were optimized to be 60 s of spectrum acquisition with 10 times average (the optimization procedure is described in Results and discussion). The part of the presented Raman spectra is given after subtracting the dichloromethane and AuMs-Ph-$C_{16}H_{33}$ spectra from the initial raw data.

The limit of detection (LOD) was calculated from the signal-to-noise ratio according to IUPAC recommendations.[49] The minimal concentration at which the signal-to-noise ratio is equal to 3 was considered as the LOD. The standard deviation (SD) of the background signal (noise) was calculated from 10 spectra of AuMs-Ph-$C_{16}H_{33}$ according to the equation:

$$\mathrm{SD} = \sqrt{\frac{\sum (x - \bar{x})}{N}}$$

where x is the intensity of the 1160 cm^{-1} characteristic Raman band, $\bar{x}$ is the mean of the measured intensities, and N is the number of measured spectra and it is found to be 19.5.

Results and discussion

The main experimental concept for an efficient microfluidic-based extraction of Ibu from water and subsequent SERS detection is presented in Fig. 1. As SERS probes, gold nanoparticles with sharp edges (AuMs) and grafted by long-chain aliphatic groups (Fig. 1A) were used. The proposed microfluidic chip includes two separate liquids, inputs for the introduction of Ibu-containing water and organic medium with dispersed SERS probes (Fig. 1B). A series of mixtures were employed in the chip design with the aim of inducing the formation of dichloromethane bubbles and efficient extraction of Ibu from water to the organic phase by AuMs-Ph-$C_{16}H_{33}$ (Fig. 1C). Then, the straight microfluidic channel with a transparent top window was introduced for on-line SERS measurements.

The TEM images of pristine and grafted AuMs are presented in Fig. 2A and B. This kind of nanoparticle provides a high concentration of the electromagnetic field at the edges, due to their shape and related high SERS enhancement.[50,51] The initial experimental studies indicated that the stability of pristine AuMs in the organic phase (dichloromethane) was very low (they can be suspended by power ultrasound, but the precipitate was formed almost immediately after switching off ultrasound – Fig. 2C). Thus, the surface of AuMs was functionalized with long aliphatic chains (Ph-$C_{16}H_{33}$) *via* an aromatic diazonium salt for the preparation of their stable suspension in the organic solvent and a simultaneous increase of the nanoparticle surface affinity towards Ibu. The AuM surface modification was confirmed by Raman spectroscopy. The

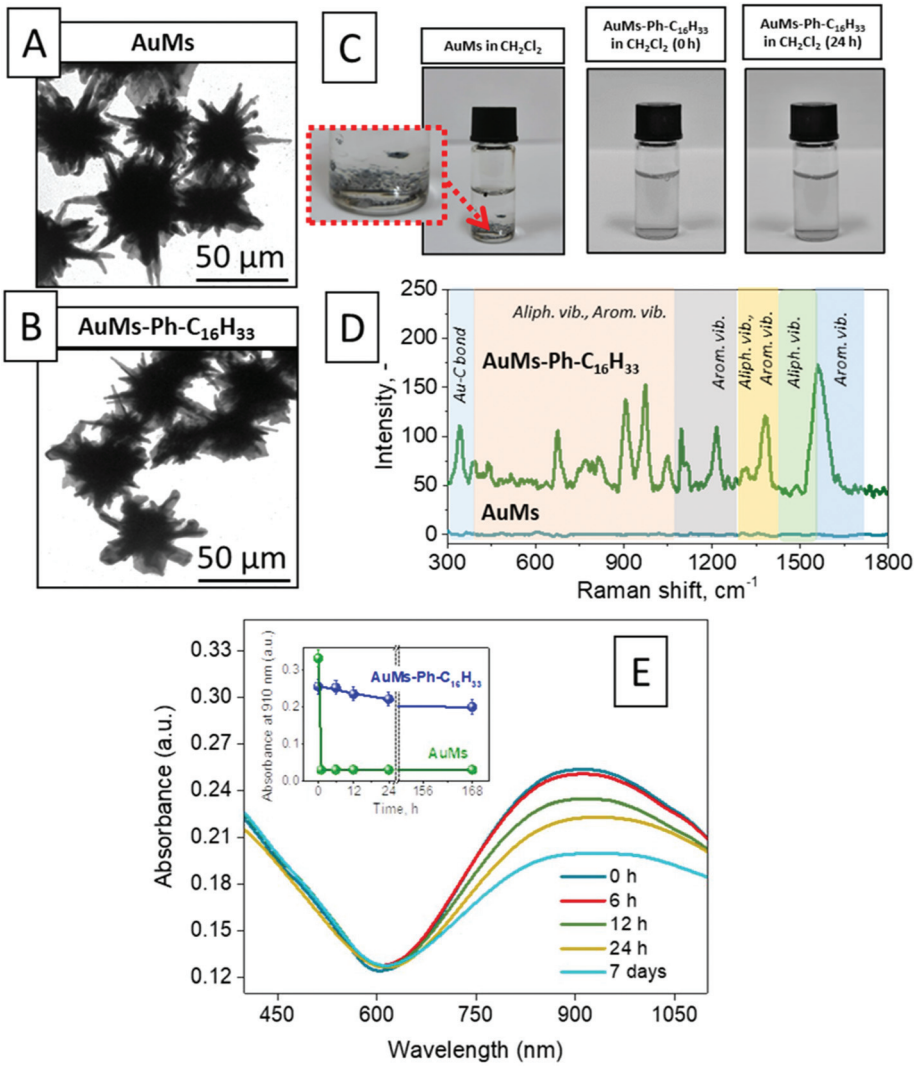

Fig. 2 (A) and (B) TEM images of AuMs before and after grafting with Ph-$C_{16}H_{33}$; (C) images of pristine and grafted AuM (after 0 and 24 h) suspensions in dichloromethane; (D) Raman spectra of AuMs measured before and after grafting with Ph-$C_{16}H_{33}$; and (E) UV-Vis spectra of the suspension of grafted AuMs in dichloromethane after different times of suspension storage (the inset shows the dependency of plasmon absorption band intensity maximum on the time of storage for pristine and grafted AuMs).

appearance of the characteristic vibration bands of aliphatic ($C_{16}H_{33}$) and aromatic (C_6H_4) chemical moieties indicates the successful grafting of the nanoparticle surface (Fig. 2D). The control TEM measurements indicate the conservation of the AuM structure (*i.e.*, the presence of SERS-active sharp edges) after the modification procedure (Fig. 2B). In turn, the grafting of the AuM surface with Ph-$C_{16}H_{33}$ chemical moieties results in a significant increase in their stability in the dichloromethane phase (the corresponding images are shown in Fig. 2C). Fig. 2E shows the time-resolved UV-Vis absorption spectra (and images) recorded after different storage times of pristine or grafted AuMs in the organic phase. The broad absorption band remains almost the same for the first several days, and only after 1 week of storage, a decrease of the absorption band intensity (characteristic for AuM sedimentation) was observed.

In the next step, the proposed approach was employed for Ibu microfluidic extraction and on-line SERS detection. First, the extraction procedure was optimized by the variation of the experimental conditions and the number of employed mixers. The microfluidic extraction efficiency was estimated by the collection of organic and water phases, their separation, and identification of the amount of Ibu in the dichloromethane phase. The extraction efficiency results are presented in Fig. 3A as a function of the number of employed micromixers. The results show that 5 micromixers are enough to reach 95% extraction efficacy of Ibu from water to the organic phase (since the volume of introduced dichloromethane was three times lower than the water volume, the obtained value corresponds to *ca.* 300 value of the preconcentration factor). In the next step, we employed the addition of SERS tags into the organic phase (without Ibu presence in water) and determined

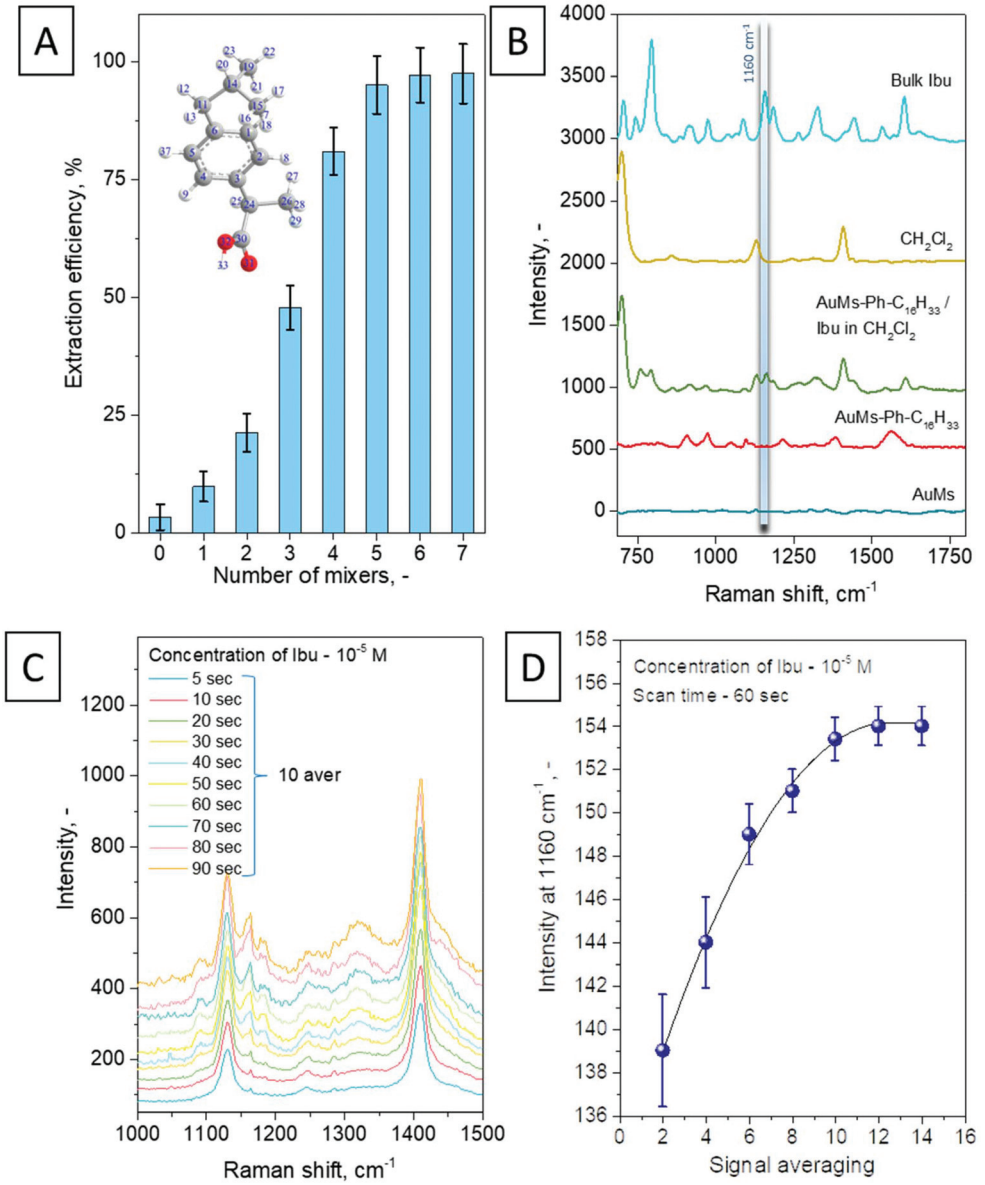

Fig. 3 (A) Dependency of the Ibu extraction efficiency on the number of microfluidic mixers in chip design; (B) Raman spectra of bulk Ibu and dichloromethane, SERS spectrum of grafted AuMs-$C_{16}H_{33}$, and SERS spectra of Ibu (extracted to dichloromethane, 10^{-4} initial concentration in water), measured in the microfluidic regime; optimization of microfluidic SERS measurement conditions: (C) dependency of the raw spectral intensity on acquisition time, and (D) characteristic Ibu peak intensity dependence on spectral averaging.

the additional SERS signal arising from the presence of aliphatic chains and dichloromethane (Fig. 3B). As could be expected, both compounds produce characteristic features in Raman spectra. Some of their characteristic Raman peaks overlapped with the peaks from bulk Ibu (Fig. 3B), but fortunately, several Ibu peaks (for example – 1160 cm^{-1} one) are exclusive and can be potentially utilized for its identification (Table 1). To suppress non-informative signals from the solvent or aliphatic chains grafted to the AuM surface and obtain clearer spectral information, the SERS spectra were subjected to baseline correction by subtracting the Raman response of the solvent and aliphatic groups.

The proposed approach of Ibu detection may be sensitive to the time and conditions of spectral data collection since the SERS measurements are performed in the on-line flow regime and the excitation laser spot is alternatively focused on water or dichloromethane bubbles. To prevent potential measurement errors and increase the method reliability, we further optimize the time of SERS spectrum acquisition (Fig. 3C shows the raw SERS spectra as a function of acquisition time) and averaging (Fig. 3D shows the intensity of the characteristic Ibu band as a function of spectral averaging). The optimal conditions were found to be 60 s for spectrum collection (this time corresponds to the saturation of the characteristic Ibu

Table 1 The affiliation of characteristic Ibu, CBZ and Cel Raman peaks

Wave numbers (cm^{-1})	Approximate descriptions	Wave numbers (cm^{-1})	Approximate descriptions
Ibuprofen			
704	C–OH stretch; C^3–C^{24} stretch; C–O out-of-plane wagging; ϕ out-of-plane bending; ϕ out-of-plane bending	1160	$C^{15}H_3$ rocking; $C^{19}H_3$ rocking; C^{11}–C^{14} stretching
743	CH_3 rocking; ϕ CH out-of-plane bending	1184	C_6–C_{11} stretching
795	Out-of-plane bending; CH_3 rock; C–O out-of-plane wagging	1264	C^{24}–H^{25} bending; (CO–H in-plane bending)
920–923	CH out-of-plane bending; $C^{15}H_3$ rocking (CO–H bending (H-bonded))	1322	In-plane bending (3); C^{24}–H^{25} bending + CO–H in-plane bending
975	$C^{26}H_3$ rocking; C^{26}–C^{24}–C^{30} antisymmetric stretching	1443	CH_2 deformation; $C^{15}H_3$ and $C^{19}H_3$ antisymmetric deformation
1087	$C^{15}H_3$ rocking; $C^{14}(C^{11}C^{15}C^{19})$ antisymmetric stretching	1605	C–C stretching
Celecoxib[52,53]			
860–970	N–S stretching in the SO_2NH_2 group, C–H out-of-plane bending vibrations	1134, 1168	NH_2-rocking and symmetric stretching of the SO_2 group
1032	C–H in plane bending vibrations	1206	C–F stretching vibrations
Carbamazepine[52–54]			
1134	C–C stretching; N–H bending in carboxamide groups	1329, 1480, 1620	C–H bending; C–C stretching
1198	N–H bending	1597	N–H bending; O–H bending
1552	C–C stretching	1289	C–H bending

peak intensity and the passage of approximately 90 dichloromethane drops through the area of SERS signal collection) and 10 spectral averaging. Under these conditions, the Ibu characteristic band intensity deviation, calculated as a ratio of measurement standard deviation to characteristic peak intensity, does not exceed 3.5% (Fig. 3D), still with an acceptable signal-to-noise ratio. These parameters make the measurements semiquantitative. Further increase of the acquisition time or spectral averaging does not significantly affect the measurement accuracy. Thus, 60 s and 10 spectral averaging were subsequently used in all further experiments. The obtained optimal parameters of SERS measurements also allow us to calculate the water volume required for the relevant detection of IBU. Taking into account the water feed rate in the microfluidic chip, 3 ml is the optimal value. On the other hand, the required water volume can be decreased by changing the microfluidic chip parameters, *i.e.*, the decrease of channel size, with the related decrease of the water feed rate.

In the next step, we performed microfluidic extraction and SERS recognition of Ibu from its model water solutions with various Ibu concentrations, from saturated (10^{-4} M) up to nanomolar (10^{-8} M) ones. The obtained results (after spectral subtractions) are presented in Fig. 4A. As could be expected, the decrease of the initial Ibu concentration in water leads to a corresponding reduction of the characteristic SERS peak intensities. For the quantification of analysis and calibration curve creation, we chose the more pronounced Ibu peak, located at 1160 cm^{-1}, as a characteristic one and plotted its intensity against the logarithm of the initial Ibu concentration in water. The obtained dependence in a 10^{-4}–10^{-8} M concentration range, presented in Fig. 4B, is close to a linear one with a correlation coefficient of 0.97. On the base of this dependency and the value of spectral noise (19.5 – see the Experimental section for details), we calculated the limit of detection (LOD) of Ibu to be 1.2×10^{-8} M.

For the estimation of the proposed approach reproducibility, Ibu detection was performed with several microfluidic chips and independently prepared and grafted AuM nanoparticles. The obtained results are presented in Fig. 4C for three Ibu concentrations. The deviation between independent measurements in the framework of a single chip, between different chips, or with the utilization of different Ibu concentrations does not exceed 3.6%. A comparison of the obtained measurement uncertainty with typical errors shown in Fig. 4B allows us to claim that by the proposed method it is possible to determine the Ibu concentration with one order of magnitude accuracy. Finally, we also demonstrate the possibility of microfluidic chip regeneration. For this purpose, the subsequent detection of different Ibu concentrations (from higher to lower ones) was performed in one single microfluidic chip (Fig. 4D). Between the measurements, the chip was recovered by washing with dichloromethane in the flow regime. In all cases, we successfully detected the presence of Ibu with the characteristic Raman intensity, corresponding well to the calibration curve (Fig. 4B *vs.* Fig. 4D).

In our previous experiments, we used distilled water. In real samples, however, a complex matrix can be expected, complicating the detection procedure. On the other hand, most of the side compounds present in wastewater are water-soluble and have lower solubility in the organic phase, which prevent their extraction and elimination of undesired SERS signal interference. To demonstrate the applicability of the developed SERS tags for complex samples, we performed a range of experiments, attempting on Ibu detection in simulated real samples. The simulated solution containing NaCl (0.9%, corresponding to water contamination by inorganic ions as well as to the composition of the physiological solution), water-soluble biomolecules (bovine serum albumin (BSA) as a model compound), and water with various pH values was used. The obtained Raman spectra are shown in Fig. 5A (after

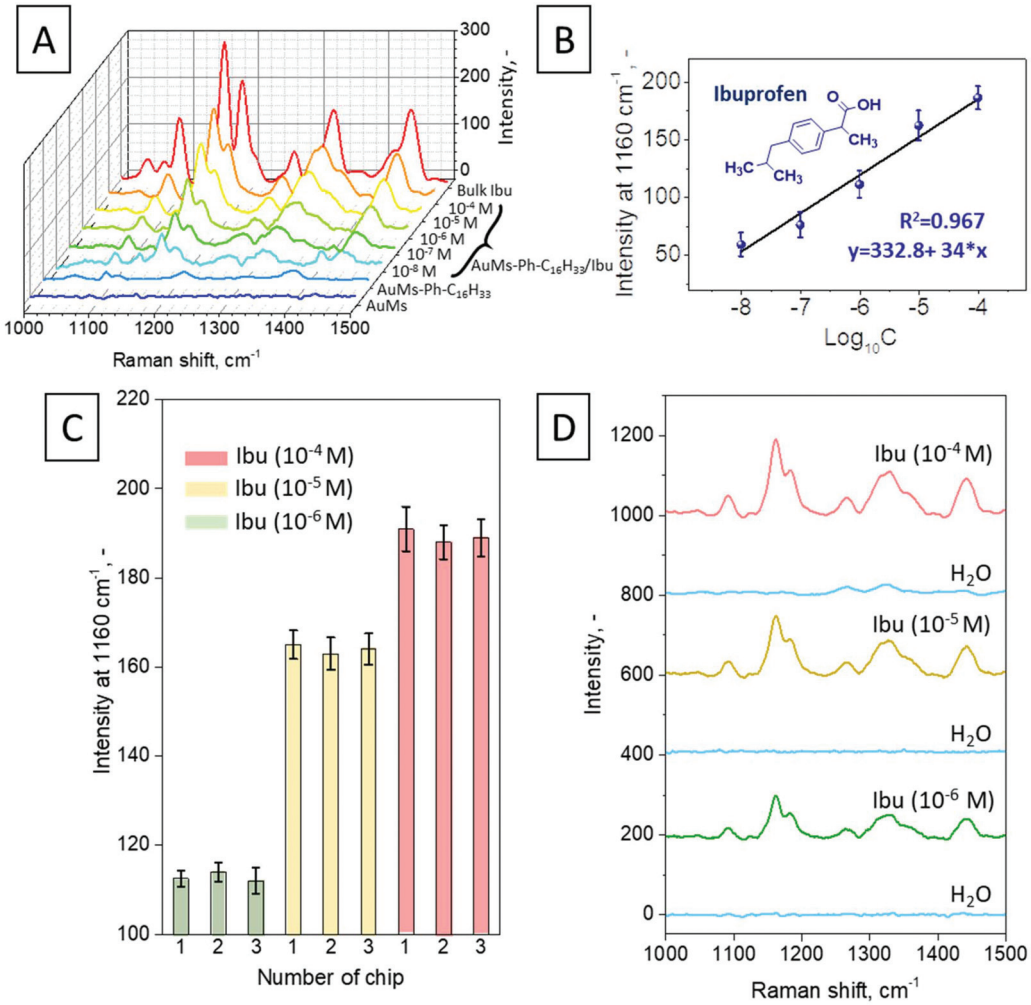

Fig. 4 (A) SERS spectra of Ibu measured in the on-line regime after dissolving Ibu in water (concentrations range from 10^{-4} to 10^{-8}) and microfluidic extraction in dichloromethane with dispersed AuMs-$C_{16}H_{33}$ (spectra are given after the subtraction of the signal from dichloromethane and Ph-$C_{16}H_{33}$; (B) dependency of the characteristic Ibu peak intensity on its initial concentration in water; (C) test of reproducibility – intensities of the characteristic Ibu SERS band measured on three different chips; and (D) microfluidic chip regeneration through subsequent SERS detection of various Ibu concentrations and intermediate chip regeneration.

subtraction of the spectra of dichloromethane and Ph-$C_{16}H_{33}$) and compared with the SERS spectra of Ibu dissolved in distilled water. For better clarity, we also plotted the intensity of the characteristic Ibu peak against the measurement conditions (Fig. 5B). As is evident, the presence of inorganic ions (sample designated as a physiological solution) results in a slight decrease in the characteristic peak intensity by *ca.* 20%. In this case, we observed the partial agglomeration of AuMs on the water/dichloromethane interface, which apparently led to a decrease of the effective SERS tag concentration in the organic phase and the corresponding decrease of Ibu detection ability. However, the overall spectral features as well as the characteristic peaks remain well visible and sufficient for Ibu identification. Even better results were observed in the case of BSA addition. In this case, the AuM agglomeration does not occur, only Ibu molecules are extracted into the organic phase, and the perfect conservation of the characteristic peak intensity (in comparison with distilled water) was observed. Therefore, the presence of water-soluble biomolecules, which could produce significant spectral noise and offset the SERS benefits, absolutely does not interfere with the proposed detection method. However, changes in pH were found to affect the SERS signal pronouncedly. In this case, the carboxylic group in the Ibu structure can be protonated or deprotonated, determining in this way the Ibu solubility and its distribution between the water and organic phases. Thus, at increased pH, the Ibu extraction and subsequent detection were significantly restricted. At the acidic pH, an increase by 11% of the characteristic peak intensity (in comparison with distilled water – neutral pH) was observed. Therefore, the results indicate that the proposed approach allows the detection of Ibu at the background of biomolecules or in the presence of inorganic ions with the necessity to keep the analytical solution pH at a neutral or acidic level.

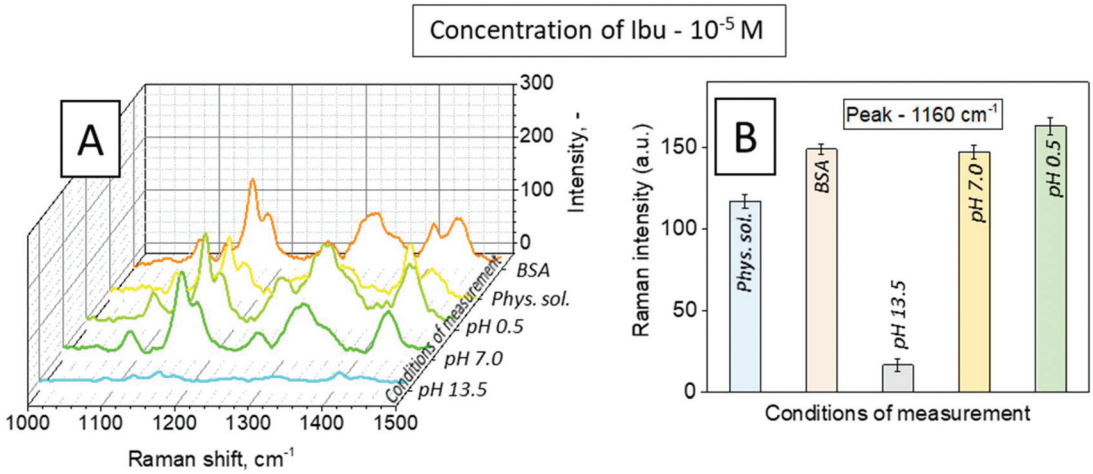

Fig. 5 (A) SERS spectra measured in the on-line regime after microfluidic extraction of Ibu from water, containing "inorganic ions", BSA or from water with different pH values and (B) characteristic Ibu SERS peak intensity as a function of initial water content.

In the next step, we demonstrate the ability of additional lipophilic pharmaceutical detection – carbamazepine and celecoxib (Fig. 6). First, we check the ability to extract both compounds from water to the dichloromethane phase using the proposed mixing design. Dependencies of extraction efficiency on the number of mixtures in the microchip design for both compounds are presented in Fig. 6A and D. As is evident, and like the Ibu case, the five mixtures were fully enough to extract most of the compounds from water to the organic phase. In the next step, we performed the *in situ* SERS detection of both compounds in the microfluidic regime in a similar manner to the Ibu experimental route. The obtained results are presented in Fig. 6B and E (Raman spectra after subtraction of the signal from dichloromethane) and Fig. 6C and F (calibration curves). As is evident, better results were obtained in the celecoxib case, where the spectral pattern is maintained with an acceptable resolution up to a 10^{-8} M level of the initial concentration. Slightly worse results were obtained in the case of carbamazepine, where some degree of merging of peaks potentially complicated the detection procedure. In addition, the calibration curve slope for celecoxib shows a larger value than that for carbamazepine, indicating that the sensitivity of the proposed approach can vary from one pharmaceutical to another. It may seem that this fact is a potential limiting factor in the pro-

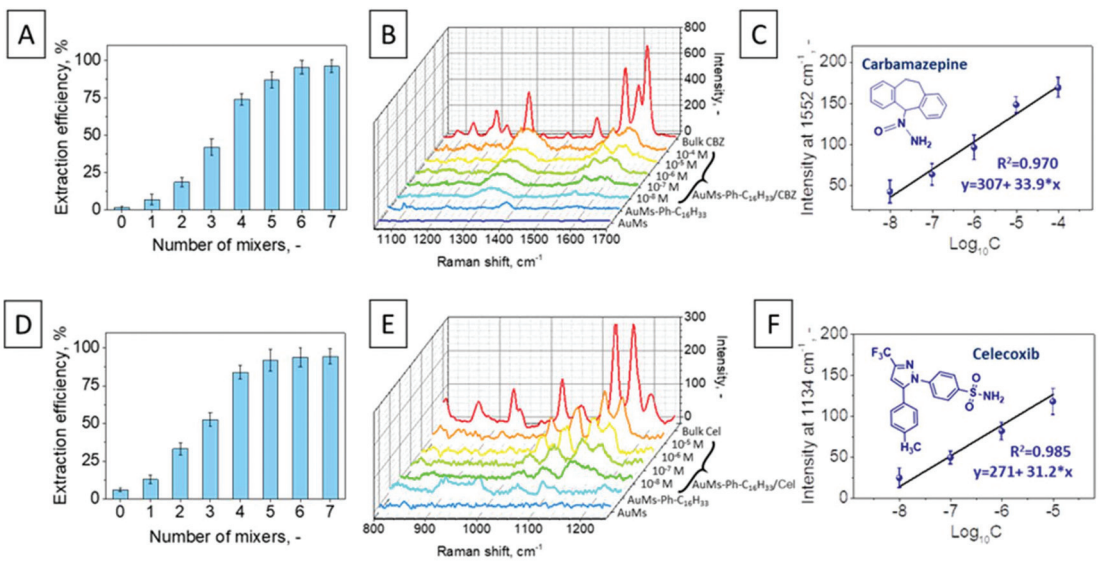

Fig. 6 (A) and (D) Dependency of the carbamazepine and celecoxib extraction efficiencies on the number of microfluidic mixers in chip design; (B) and (E) SERS spectra of carbamazepine and celecoxib measured in the on-line regime after dissolving pharmaceuticals in water (concentration range from 10^{-4} to 10^{-8}M) and microfluidic extraction to dichloromethane with dispersed AuMs-$C_{16}H_{33}$ (spectra are given after the subtraction of the signal from dichloromethane and Ph-$C_{16}H_{33}$), and (C) and (F) dependencies of the characteristic carbamazepine and celocoxib peak intensities on their initial concentrations in water.

posed method for the detection of negligibly small amounts of pharmaceuticals in water. However, the recent development of the combined approach in the analysis of SERS spectra, based on mathematical and statistical algorithms (for example – principal component analysis or artificial intelligence), allows replacing the manual spectrum interpretation by more sensitive and accurate programmable methods.[45,55,56] Therefore, it is possible that in the analysis of some antibiotics, it will be necessary to introduce additional (and automatic) algorithms for spectrum processing and interpretation.

Finally, we demonstrated the ability of pharmaceutical detection, using the proposed approach at the background of various water kinds. In particular, artificial freshwater, wastewater and water with humic acid contents were prepared according to [AdRef3, AdREf4]. CBZ and Cel were dissolved in the prepared water samples (concentrations – 10^{-4} M in both cases) and subjected to on-line SERS measurements using the proposed microfluidic extraction and detection approach. The results are presented in Fig. 7A (CBZ) and Fig. 7B (Cel). As is evident, the kind of water does not significantly affect the SERS spectral pattern received from Cel. On the other hand, some decrease of the Cel characteristic band intensity was observed, compared to previously used distilled water (Fig. 7C). Thus, for performing semiquantitative analysis, the kind of water should be taken into account before deciding on the Cel amount in the measured samples. In the case of CBZ, the worst situation was observed – the peak interference occurs in addition to the relatively high signal-to-noise ratio. Thus, manual detection of CBZ can be considered as a complicated task and the utilization of advanced spectrum analysis algorithms should be considered in this case.[45,55,56] In turn, we performed experiments with different kinds of water, which allows us to demonstrate the main advantages of the proposed approach: unlike many common cases, which require the previous extraction of pharmaceuticals and their subsequent analysis by equipment-demanding techniques,[9–14] we are not limited by the presence of metal ions or other organic compounds; the detection can be performed in the framework of a single chip and requires just 10 min for complete determination of the targeted drug presence.

Finally, we evaluated the repeatability of the proposed approach at intraday and interday time intervals. For these goals, we prepared several microfluidic chips and performed the SERS detection of Ibu (10^{-4} M, water) for one day or day to day for 3 weeks. Between measurements, the chips were stored under normal laboratory conditions, without temperature or humidity control. The results of the measurements are presented in Fig. 8. In particular, Fig. 8A shows the results of measurements on three different chips (characteristic SERS band uncertainty is included as error bars for one day). In this case, we do not observe any deviation in the averaged SERS intensity. In turn, Fig. 8B shows the stability evaluation for 3 weeks (also performed with the utilization of three chips). Similarly, we do not observe any decrease of the characteristic band intensity and any measurement uncertainty increases. This result can be expected, since we used a thin gold film as a plasmonic support, and this plasmon-active metal (unlike silver) does not show the tendency to oxidize and lose plasmon activity for a long time.

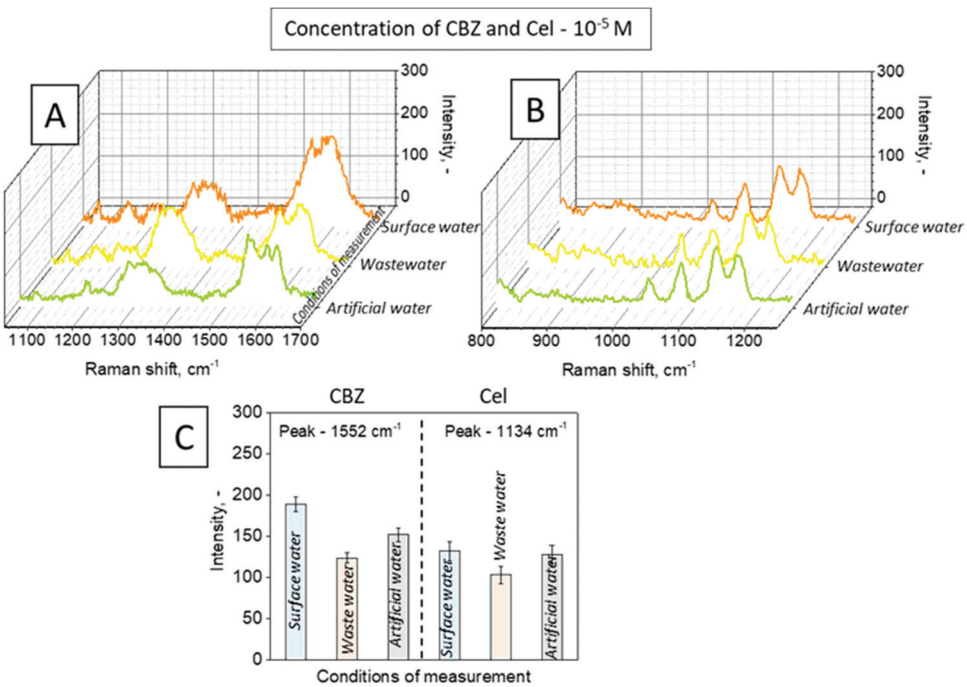

Fig. 7 (A) and (B) SERS spectra measured in the on-line regime after microfluidic extraction of CBZ and Cel from artificial freshwater, wastewater, and ground water (with humic acid addition) and (C) characteristic CBZ and Cel SERS peak intensities as a function of initial water content.

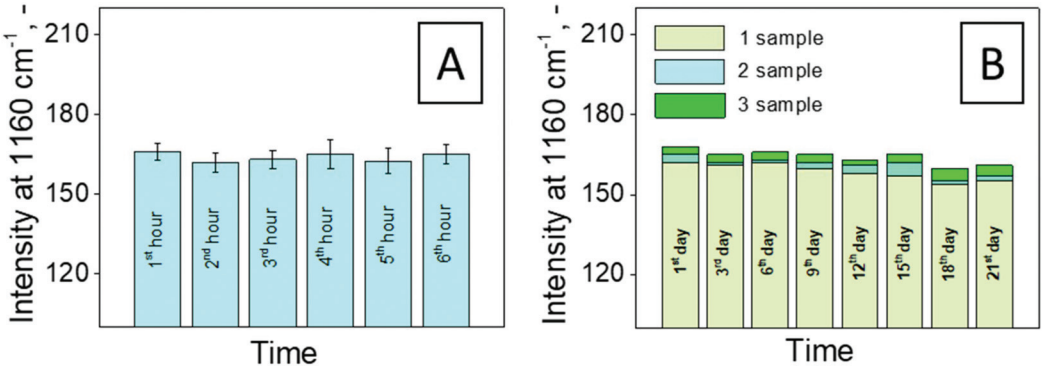

Fig. 8 Evaluation of the proposed approach stability: (A) characteristic Ibu peak intensity, measured within one day in several subsequent measurement cycles, (B) characteristic Ibu peak intensity, measured within three weeks (error bars present the signal difference between the three microfluidic chips).

Finally, it also should be mentioned that the proposed detection was performed with the utilization of a portable Raman spectrometer and simple syringe pumps, and for the creation of the microfluidic chip, the scalable 3d printing technology was used. In turn, the chemical routes for AuM synthesis and modification (grafting) are well known and repeatable. Thus, the proposed approach can be considered as simple, portative, rapid, technically undermined, and applicable for outdoor conditions. The advantages of the proposed procedure were demonstrated only for ibuprofen, as a model pharmaceutical contaminant, but it may be assumed that the same method could be used for a number of other water-insoluble drugs without the loss of its efficacy.

Conclusions

In this work, we present an alternative concept for the detection of low solublity pharmaceuticals in an rapid, online microfluidic regime. The proposed approach is based on the creation of the microfluidic chip with two inputs for the analysed water solution of the pharmaceuticals and the organic phase. The feasibility of the method was demonstrated using ibuprofen as a model pharmaceutical. The microfluidic chip was also equipped with micromixers for efficient extraction of ibuprofen and creation of dichloromethane drops. Then, SERS measurements were performed directly in the on-line microfluidic regime. As SERS tags, multibranched gold nanoparticles were added to the dichloromethane phase and the stability of AuMs was improved by surface functionalization with aliphatic chains. The proposed approach and the created device make it possible to reach close to the nanomolar detection limit level with one order of magnitude accuracy. The proposed approach was also tested on simulated contaminated water samples, with the addition of inorganic salts or model bio-contaminants. In this case, successful detection with similar resolution and accuracy was also achieved. It should be also noted that the created technique is rapid and compatible, making it suitable for out-of-door water analysis.

Conflicts of interest

There are no conflicts to declare.

Acknowledgements

This work was supported by the GACR under the project 20-03913S, Tomsk Polytechnic University Competitiveness Enhancement Program (VIU-RSCABS-194/2020).

Notes and references

1 J. L. Martinez, *Environ. Pollut.*, 2009, **157**, 2893–2902.
2 S. Rodriguez-Mozaz, S. Chamorro, E. Marti, B. Huerta, M. Gros, A. Sànchez-Melsió, C. M. Borrego, D. Barceló and J. L. Balcázar, *Water Res.*, 2015, **69**, 234–242.
3 M.-C. Danner, A. Robertson, V. Behrends and J. Reiss, *Sci. Total Environ.*, 2019, **664**, 793–804.
4 J. P. Laurenson, R. A. Bloom, S. Page and N. Sadrieh, *AAPS J.*, 2014, **16**, 299–310.
5 S. Fekadu, E. Alemayehu, R. Dewil and B. Van der Bruggen, *Sci. Total Environ.*, 2019, **654**, 324–337.
6 B. Wang, X.-L. Lv, D. Feng, L.-H. Xie, J. Zhang, M. Li, Y. Xie, J.-R. Li and H.-C. Zhou, *J. Am. Chem. Soc.*, 2016, **138**, 6204–6216.
7 J. Song, M. Huang, N. Jiang, S. Zheng, T. Mu, L. Meng, Y. Liu, J. Liu and G. Chen, *J. Hazard. Mater.*, 2020, **391**, 122024.
8 H. Wang, X. Wu, S. Yang, H. Tian, Y. Liu and B. Sun, *Food Chem.*, 2019, **286**, 322–328.
9 S. L. Z. Jiokeng, I. K. Tonle and A. Walcarius, *Sens. Actuators, B*, 2019, **287**, 296–305.
10 M. C. Campos-Mañas, I. Ferrer, E. M. Thurman, J. A. Sánchez-Pérez and A. Agüera, *Sci. Total Environ.*, 2019, **664**, 874–884.
11 D. S. Aga, M. Lenczewski, D. Snow, J. Muurinen, J. B. Sallach and J. S. Wallace, *J. Environ. Qual.*, 2016, **45**, 407–419.

12 I. Kanfer, M. F. Skinner and R. B. Walker, *J. Chromatogr., A*, 1998, **812**, 255–286.
13 C. Hao, X. Zhao and P. Yang, *TrAC, Trends Anal. Chem.*, 2007, **26**, 569–580.
14 H. C. Goicoechea, M. J. Culzoni, M. D. G. García and M. M. Galera, *Talanta*, 2011, **83**, 1098–1107.
15 K. Y. Hong, C. D. L. de Albuquerque, R. J. Poppi and A. G. Brolo, *Anal. Chim. Acta*, 2017, **982**, 148–155.
16 O. Guselnikova, P. Postnikov, A. Pershina, V. Svorcik and O. Lyutakov, *Appl. Surf. Sci.*, 2019, **470**, 219–227.
17 Y. Jiang, D.-W. Sun, H. Pu and Q. Wei, *Trends Food Sci. Technol.*, 2018, **75**, 10–22.
18 H. Tang, C. Zhu, G. Meng and N. Wu, *J. Electrochem. Soc.*, 2018, **165**, B3098.
19 C. Han, J. Chen, X. Wu, Y. Huang and Y. Zhao, *Talanta*, 2014, **128**, 293–298.
20 Y. Kalachyova, O. Guselnikova, R. Elashnikov, I. Panov, J. Žádný, V. Církva, J. Storch, J. Sykora, K. Zaruba, V. Švorčík and O. Lyutakov, *ACS Appl. Mater. Interfaces*, 2019, **11**, 1555–1562.
21 D. Deng, H. Yang, C. Liu, K. Zhao, J. Li and A. Deng, *Sens. Actuators, B*, 2019, **283**, 563–570.
22 R. Rosal, A. Rodríguez, J. A. Perdigón-Melón, A. Petre, E. García-Calvo, M. J. Gómez, A. Agüera and A. R. Fernández-Alba, *Water Res.*, 2010, **44**, 578–588.
23 S. Jones, A. Pramanik, R. Kanchanapally, B. P. V. Nellore, S. Begum, C. Sweet and P. C. Ray, *ACS Sustainable Chem. Eng.*, 2017, **5**, 7175–7187.
24 T. Frosch, A. Knebl and T. Frosch, *Nanophotonics*, 2019, **9**, 19–37.
25 A. H. Nguyen, X. Ma, H. G. Park and S. J. Sim, *Sens. Actuators, B*, 2019, **282**, 765–773.
26 H. Pu, W. Xiao and D.-W. Sun, *Trends Food Sci. Technol.*, 2017, **70**, 114–126.
27 S. Patze, U. Huebner, F. Liebold, K. Weber, D. Cialla-May and J. Popp, *Anal. Chim. Acta*, 2017, **949**, 1–7.
28 I. J. Hidi, J. Heidler, K. Weber, D. Cialla-May and J. Popp, *Anal. Bioanal. Chem.*, 2016, **408**, 8393–8401.
29 V. Burtsev, E. Miliutina, M. Erzina, Y. Kalachyova, R. Elashnikov, V. Svorcik and O. Lyutakov, *J. Phys. Chem. C*, 2019, **123**, 30492–30498.
30 K. R. Ackermann, T. Henkel and J. Popp, *ChemPhysChem*, 2007, **8**, 2665–2670.
31 C. Andreou, M. R. Hoonejani, M. R. Barmi, M. Moskovits and C. D. Meinhart, *ACS Nano*, 2013, **7**, 7157–7164.
32 W.-S. Zhang, Y.-N. Wang, Y. Wang and Z.-R. Xu, *Sens. Actuators, B*, 2019, **283**, 532–537.
33 O. Durucan, K. Wu, M. Viehrig, T. Rindzevicius and A. Boisen, *ACS Sens.*, 2018, **3**, 2492–2498.
34 S. Patze, U. Huebner, F. Liebold, K. Weber, D. Cialla-May and J. Popp, *Anal. Chim. Acta*, 2017, **949**, 1–7.
35 I. J. Hidi, A. Mühlig, M. Jahn, F. Liebold, D. Cialla, K. Weber and J. Popp, *Anal. Methods*, 2014, **6**, 3943–3947.
36 I. J. Hidi, J. Heidler, K. Weber, D. Cialla-May and J. Popp, *Anal. Bioanal. Chem.*, 2016, **408**, 8393–8401.
37 N. D. Kline, A. Tripathi, R. Mirsafavi, I. Pardoe, M. Moskovits, C. Meinhart, J. A. Guicheteau, S. D. Christesen and A. W. Fountain, *Anal. Chem.*, 2016, **88**, 10513–10522.
38 Z. Lao, Y. Zheng, Y. Dai, Y. Hu, J. Ni, S. Ji, Z. Cai, Z. J. Smith, J. Li, L. Zhang, D. Wu and J. Chu, *Adv. Funct. Mater.*, 2020, **30**, 1909467.
39 M. Mao, B. Zhou, X. Tang, C. Chen, M. Ge, P. Li, X. Huang, L. Yang and J. Liu, *Chem. – Eur. J.*, 2018, **24**, 4094–4102.
40 O. Guselnikova, Y. Kalachyova, K. Hrobonova, M. Trusova, J. Barek, P. Postnikov, V. Svorcik and O. Lyutakov, *Sens. Actuators, B*, 2018, **265**, 182–192.
41 M. Sugiyama, S. Wu, K. Hosoda, A. Mochizuki and T. Hori, *Limnol. Oceanogr.: Methods*, 2016, **14**, 343–357.
42 Synthetic Wastewater Preparation, http://zelalabwork.blogspot.com/2013/03/synthetic-wastewater-preparation.html, (accessed March 31, 2021).
43 S. J. Boggs, D. Livermore and M. G. Seitz, *Humic substances in natural waters and their complexation with trace metals and radionuclides: a review. [129 references]*, Argonne National Lab., IL (USA), 1985.
44 A. Rodrigues, A. Brito, P. Janknecht, M. F. Proença and R. Nogueira, *J. Environ. Monit.*, 2009, **11**, 377–382.
45 M. Erzina, A. Trelin, O. Guselnikova, B. Dvorankova, K. Strnadova, A. Perminova, P. Ulbrich, D. Mares, V. Jerabek, R. Elashnikov, V. Svorcik and O. Lyutakov, *Sens. Actuators, B*, 2020, **308**, 127660.
46 J. Kumirska, A. Plenis, P. Łukaszewicz, M. Caban, N. Migowska, A. Białk-Bielińska, M. Czerwicka and P. Stepnowski, *J. Chromatogr. A*, 2013, **1296**, 164–178.
47 S. Ahuja, *J. Pharm. Sci.*, 1976, **65**, 163–182.
48 P. Kusch, *Gas Chromatography - Derivatization, Sample Preparation, Application*, 2019.
49 D. Rustichelli, S. Castiglia, M. Gunetti, K. Mareschi, E. Signorino, M. Muraro, L. Castello, F. Sanavio, M. Leone, I. Ferrero and F. Fagioli, *J. Transl. Med.*, 2013, **11**, 197.
50 J.-J. Li, C. Wu, J. Zhao, G.-J. Weng, J. Zhu and J.-W. Zhao, *Spectrochim. Acta, Part A*, 2018, **204**, 380–387.
51 S. Barbosa, A. Agrawal, L. Rodríguez-Lorenzo, I. Pastoriza-Santos, R. A. Alvarez-Puebla, A. Kornowski, H. Weller and L. M. Liz-Marzán, *Langmuir*, 2010, **26**, 14943–14950.
52 O. Guselnikova, A. Trelin, A. Skvortsova, P. Ulbrich, P. Postnikov, A. Pershina, D. Sykora, V. Svorcik and O. Lyutakov, *Biosens. Bioelectron.*, 2019, **145**, 111718.
53 F. Lussier, V. Thibault, B. Charron, G. Q. Wallace and J.-F. Masson, *TrAC, Trends Anal. Chem.*, 2020, **124**, 115796.
54 G. Socrates, *Infrared and Raman characteristic group frequencies: tables and charts*, John Wiley & Sons, 2004.
55 B. Vijayakumar, V. Kannappan and V. Sathyanarayanamoorthi, *J. Mol. Struct.*, 2016, **1121**, 16–25.
56 W. Czernicki and M. Baranska, *Vib. Spectrosc.*, 2013, **65**, 12–23.

